

Local morphological pattern: A scale space shape descriptor for texture classification

Swalpa Kumar Roy ^{a,*}, Bhabatosh Chanda ^b, Bidyut B. Chaudhuri ^c, Dipak Kumar Ghosh ^d, Shiv Ram Dubey ^e

^a Department of Computer Science & Engineering, Jalpaiguri Government Engineering College, Jalpaiguri-735102, India

^b Electronics & Communication Sciences Unit, Indian Statistical Institute, Kolkata-700108, India

^c Computer Vision & Pattern Recognition Unit, Indian Statistical Institute, Kolkata-700108, India

^d Department of Electronics and Communication Engineering, Adamas University, Kolkata-700126, India

^e Computer Vision Group, Indian Institute of Information Technology, Sri City, Chittoor, Andhra Pradesh-517646, India

ARTICLE INFO

Article history:

Available online xxxx

Keywords:

Local shape vector (Lsv)
Local morphology pattern (LMP)
Morphology scale-space
Texture classification

ABSTRACT

This work sheds light on real world texture classification problem where textural information present at several scales as images are captured from different distances and zooming conditions. Inspired by the concept of mathematical morphology in image analysis, we developed a novel statistical approach to texture representation, which yields more discriminative, simple, efficient, yet robust descriptor called local morphology pattern (LMP). The proposed approach consists of two parts: first it generates a morphological scale space representation of the texture image, called local shape vector (Lsv) using two commonly used powerful morphology operations namely, “opening” and “closing” at different scale. It perfectly localizes and well preserves the contours information of the objects. Then LMP is formed by utilizing the relation of center pixel with its neighboring pixels in the scale space. The encoding of LMP is done via uniform pattern scheme. The normalized histogram of LMP (HLMR) is computed by concatenating the histograms of LMP at different scales. It is observed that LMP is invariant under local Lipschitz transform and its extension is adequate to precisely differentiate between the fundamental texture primitives. Lipschitz is a very conventional transform which incorporates rotation, translation, projective transformation and also changes in view-point. Extensive experiments of texture classification on the benchmark texture databases Outex_TC-00010 (Outex_TC10), Outex_TC-00012 (Outex_TC12), KTH-TIPS, and UIUC validate that the proposed LMP descriptor has better or comparable performance with well-known and state-of-the-art methods.

© 2018 Elsevier Inc. All rights reserved.

1. Introduction

Texture provides a rich visual representation in the image surfaces, since it often exhibits intensity variations with certain repeated patterns. Texture Analysis is a powerful approach for many applications in the field of computer vision and pattern classifications such as object recognition, material classification, natural scene identification, segmentation [1,2] and iris recognition [3]. It has been extensively studied in the past two decades due to its importance in understanding of texture recognition process in human as well as its suitable role plays in the field of computer

vision. Although for human it is easy to identify texture primitives, yet it poses challenges in computer vision because the picture may be captured under different scale, varying illumination, uncontrolled environments, with changing viewpoint, etc. A good texture description should address illumination, rotation and scale variations. Earlier texture classification methods mainly concentrate on the statistical analysis of texture images. In recent literature, two categories of texture classification approaches dominate current research, namely texture descriptor based methods [4–6] and deep learning based methods [7–11]. In deep learning based methods a Convolutional Neural Network (CNN) have been proposed and trained to classify the texture images [12,9]. The deep learning based methods offer good classification performance, however it has the following limitations: it requires a large amount of data and it is computationally expensive to train. The complex models take weeks to train using several machines equipped with expensive GPUs. Also, at present, no strong theoretical foundation to

* Corresponding author.

E-mail addresses: swalpa@cse.jgec.ac.in (S.K. Roy), chanda@isical.ac.in (B. Chanda), bbc@isical.ac.in (B.B. Chaudhuri), dipak@ieee.org (D.K. Ghosh), srdubey@iiits.in (S.R. Dubey).

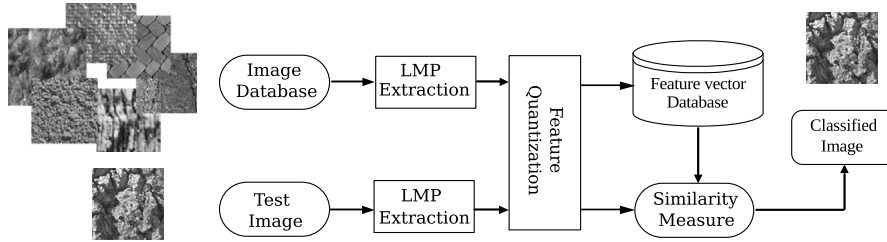


Fig. 1. Texture classification framework using proposed LMP.

finding the topology/training method/flavor/hyper-parameters for deep learning exist in the literature. On the other hand, the descriptor based methods have the advantage of easy to use, data independence, and robustness to real-life challenges such as illumination and scale differences. Therefore, the design of effective texture descriptor is regarded as extremely important for texture recognition.

Kashyap and Khotanzad [13] were first to introduce a circular autoregressive approach for rotation invariant texture classification. Later on, many models are introduced to achieve rotation and grey scale transform invariant texture classification, such as hidden Markov model [14], Gaussian Markov random field [15], and multi-resolution [16] analysis. It is more difficult to achieve the scale invariance as compared to grey scale transform and rotation invariance. Therefore, researchers attempt to bring off local and global scale invariant features. Varma and Garg [17] extracted a local fractal dimension for each pixel and then computed a statistical histogram. Liu and Fieguth [18] applied random projection for densely sampled image patches and then extracted histogram or signature feature. Han and Ma [19] computed the first and second order statistical features after summing up all the Gabor filter responses for each pixel with multiple scales but along the same orientation. Zhang et al. [20] detected Harris and Laplacian regions and extracted signature over the normalized regions instead of entire image pixels. Since local scale normalization is computationally slow, global scale invariant feature extraction method drew attention to vision community. To resist variations in scale, Yao and Sun [21] introduced statistical normalized edge feature distribution. Hui et al. [22] used Laplacian blob to estimate a global scale and they extracted wavelet spectrum feature after image normalization. Xu et al. [23,24] classified the pixels in the image into multiple point set by gray intensities or local feature descriptors. Then, a global fractal dimension was computed for each point set and a vector was formed by concatenating this fractal dimension. Crosier and Griffin [25] extracted multi-scale BIF features and used pyramid histogram with shifting matching scheme. However, shifting matching scheme is computationally expensive.

In order to gain more robustness, feature extraction is often performed over local region of the image. In 1996 a computationally efficient texture descriptor, called local binary pattern (LBP) was proposed by Ojala et al. [26,27] for gray-scale and rotation invariant texture classification. The LBP based models have achieved impressive texture classification results and are widely used in other domain too, such as texture segmentation, face recognition, shape localization and object recognition [28]. Many variants of LBP have been proposed very recently such as dominant LBP [29], LBP variance [30], extended LBP [31], completed LBP [5], local ternary pattern (LTP) [32], order-based local descriptor [33], local wavelet pattern [34], multichannel decoded LBP [35], a complete dual-cross pattern (CdcP) [53], and local direction ZigZag pattern (LDZP) [48]. However, most of them are based on the same idea of LBP and only extracts isotropic micro structure of the image which is not enough to describe the texture information. These methods could not address the scale variation issues as well. Scale invariant tex-

ture classification is a challenging and active research topic. To address the scale variation issues, Ojala et al. [27] combined the limited number of neighboring sample points and radius to form multiresolution LBP. At the same time, the stability of LBP values deteriorates rapidly with increasing radius. Its reason is that the neighboring sampling points have less correlation with the referenced pixel when the radius is large. Li et al. [36] found an optimal scale for each pixel and then extracted the LBP feature with this scale. Yet, it is unable to extract accurate and consistent scale for all pixels. Global fractal feature based on multiscale LBP is introduced by Quan et al. [6]. However, the performance of fractal based classifiers has often lagged behind the state-of-the-art methods because when image size is small, the global fractal feature are not robust enough. To the best of our knowledge, LBP descriptor alone could not get good performance for the classification of texture with significant scale variations.

Texture features vary with the scale at which the image is captured and it is difficult to ensure that a test image has the same scale with target image. The existing texture patterns are well discriminative but have weaker invariance. This inspires us to develop a robust non-linear scale space statistical model to integrate such image patterns into a global feature that enjoys both robustness and discriminativeness. This work is motivated by the observation that the spatial distribution of local image patterns preserves its essential shape characteristics and eliminating irrelevancies. Such shape based characteristics can be well described by the so called mathematical morphology. In this paper, we proposed an effective novel descriptor to characterize the spatial distribution of local image patterns using multi-scale morphology analysis for texture classification. The LMP is globally invariant under *Lipschitz transform* (see Definition in A.1), a very general transform which incorporates rotation, translation, projective transformation (viewpoint changes), and general texture surface deformations. The extracted features encode the local image texture with suitable scale. The schematic diagram of proposed LMP based texture classification framework is shown in Fig. 1. The performance of the proposed descriptor is evaluated on three benchmark texture databases, namely Outex_TC-00010 (Outex_TC10), Outex_TC-00012 (Outex_TC12) [4], KTH-TIPS [37], and UIUC [38]. Proposed approach has demonstrated excellent performance in comparison with the existing state-of-the-art approaches.

The rest of this paper is organized as follows, Sec. 2 provides brief revisits of image morphology operations. Sec. 3 is devoted to the proposed LMP descriptor. Sec. 4 presents the scheme of feature distribution matching. The performance evaluation is reported in Sec. 5 and the conclusion is drawn in Sec. 6.

2. Local morphology operator

Developed by Serra [39], mathematical morphology is a commonly used and recognized technique in the field of image processing and computer vision [40]. In set theoretic based shape oriented approach, the image is usually treated as a set and the kernel of operation, called structuring element (SE), as another set.

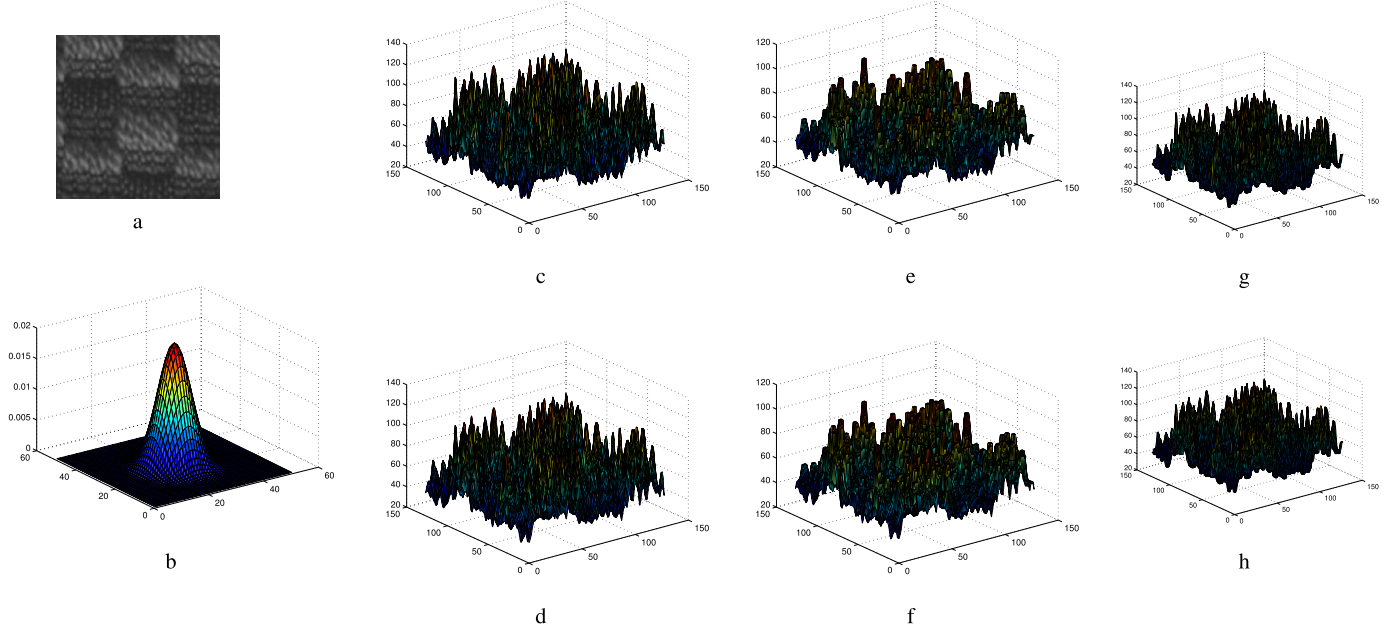


Fig. 2. (a) Original sample of texture image. (b) Surface of 0th order anisotropic Gaussian Kernel. (c) Texture surface of original image. (d) Texture surface after performing convolution with anisotropic kernel. (e)–(f) Texture surface after performing opening and closing by (3×3) SE with original image. (g)–(h) Texture surface after performing opening and closing by (3×3) SE with filtered image.

Mathematical morphology is basically set-theoretic operations between the image and SE. It can be performed using *dilation*, *erosion*, *opening*, and *closing*, etc. and can be utilized for detecting, extracting, modifying, and manipulating features from the image with given size and shape. The shape and size of the SE play an important role in morphology. Therefore, it is chosen based on the requirement of the associated application. In grey scale morphology [39], the *dilation* operation replaces a pixel gray value by the weighted maximum of its neighborhood pixel gray values, and this operator is represented as \oplus . Similarly, the gray scale erosion operation replaces a pixel gray value by the weighted minimum of its neighborhood pixel gray values and this operator is represented by \ominus . The gray scale dilation and erosion of $f(r, c)$ with $(r, c) \in \mathbb{R}^2$ by a set of points $\psi \in \mathbb{R}^2$ are defined as follows:

$$\begin{aligned}(f \oplus \psi)(r, c) &= \max\{f(r - k, c - l) | (k, l) \in \psi\} \\ (f \ominus \psi)(r, c) &= \min\{f(r + k, c + l) | (k, l) \in \psi\}\end{aligned}\quad (1)$$

where the dilation is extensive operator $(f \oplus \psi)(r, c) \geq f(r, c)$ and the erosion is anti-extensive operator $(f \ominus \psi)(r, c) \leq f(r, c)$. The structural *opening* (\circ) operation is performed through an erosion followed by a dilation and is often denoted as $f \circ \psi = (f \ominus \psi) \oplus \psi$. In reverse, the structural *closing* (\bullet) operation is performed through a dilation followed by an erosion, is denoted as $f \bullet \psi = (f \oplus \psi) \ominus \psi$. Fig. 2 shows surface representation of an texture sample (Fig. 2(c)) and filtered texture (Fig. 2(d)), and their opening (Fig. 2(e)–(f)) and closing (Fig. 2(g)–(h)). These operations form the basis of many other processes in mathematical morphology [39]. While processing the image, even the structural element ψ takes care of the shape of the features but for different sizes it cannot treat same shape objects equally. For processing different texture patterns based on their shape and size, along with the structuring element we incorporate a second attribute which is its *scale*. If the set expressing the SE is convex, the n th homothetic of the SE is produced by dilation of the SE with itself $(n - 1)$ times, keeping its shape unchanged. A SE can process the image features based on its higher order homothetics shape and size. Morpho-

logical operations with such scalable SE's are termed as *multiscale morphology* [39,41]. Given this kind of scalable structuring functions ${}^n\psi$ we can redefine the dilation and erosion operation as $F^\oplus(r, c) = (f \oplus {}^n\psi)$ and $F^\ominus(r, c) = (f \ominus {}^n\psi)$, where $F^\oplus(r, c)$ and $F^\ominus(r, c)$ represent the morphological scale-space for gray scale dilation and erosion, respectively. Morphological opening and closing with variable shape and size SEs generate a scale space representation of shape feature. Multi-scale opening and closing are defined here as follows,

$$\begin{aligned}(f \circ {}^n\psi)(r, c) &= \begin{cases} ((f \ominus {}^n\psi) \oplus {}^n\psi)(r, c) & \text{if } n > 0 \\ f(r, c) & \text{if } n = 0 \end{cases} \\ (f \bullet {}^n\psi)(r, c) &= \begin{cases} ((f \oplus {}^n\psi) \ominus {}^n\psi)(r, c) & \text{if } n > 0 \\ f(r, c) & \text{if } n = 0 \end{cases}\end{aligned}\quad (2)$$

where n represents a positive integer scale factor of the SE ψ . However, the opening $(f \circ {}^n\psi)$ for a large scale value of n , creates some large flat plateaus having similar shaped like ${}^n\psi$. Similarly the closing $(f \bullet {}^n\psi)$ creates large flat sinks shaped like ${}^n\psi$. We can implement Eqn. (2) more efficiently as

$$\begin{aligned}(f \circ {}^n\psi)(r, c) &= [(\underbrace{(f \ominus \psi) \ominus \dots \ominus \psi}_{n \text{ times}}) \oplus \underbrace{\psi \oplus \psi \dots \oplus \psi}_{n \text{ times}}](r, c) \\ (f \bullet {}^n\psi)(r, c) &= [(\underbrace{(f \oplus \psi) \oplus \dots \oplus \psi}_{n \text{ times}}) \ominus \underbrace{\psi \ominus \psi \dots \ominus \psi}_{n \text{ times}}](r, c)\end{aligned}\quad (3)$$

The n th convex homothetic structuring element (SE) ψ is obtained by recursively dilating ψ with itself $n - 1$ times as

$${}^n\psi = \psi \overbrace{\oplus \psi \oplus \psi \dots \oplus \psi}^{n-1 \text{ times}}\quad (4)$$

In natural image classification problem the scale and intensity of a particular object play an important role to evaluate its class membership. To deal with the natural image containing different shape and size objects is an interesting aspect of texture classification. Toward this goal, we develop a local shape based descriptor, called local morphological pattern (LMP) with multi-scale

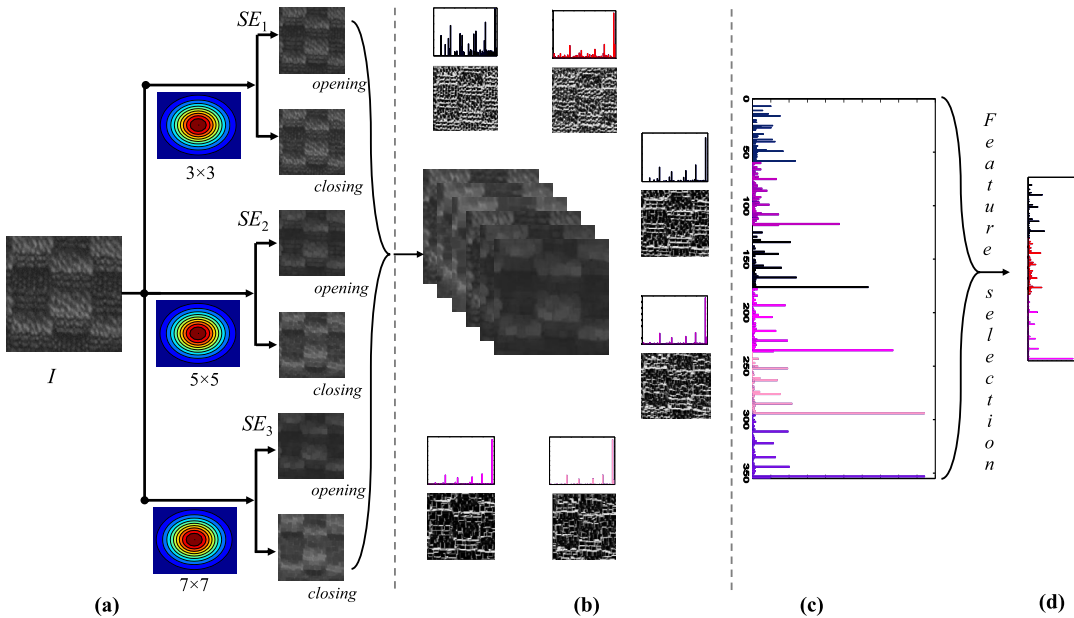


Fig. 3. Proposed local morphology pattern (LMP) feature extraction framework: (a) morphological scale space of a sample texture image derived from morphological “opening” and “closing” operators with structuring element of sizes 3×3 , 5×5 , and 7×7 ; (b) morphological tower Mt , LMP images, and their corresponding normalized histogram; (c) normalized LMP feature vector formed by concatenating all the normalized histogram; (d) selected dominant LMP feature.

shape representation. Shape of an image carries information about gray intensity or any other finite signal which can be viewed as an object conveying some textural information. In this context, scale represents the smallest size of a shape pattern that can accommodate within the image. Linear scale space approach is achieved by convolving the local image patch with a Gaussian kernel of standard deviation σ , or local weighted average of span $\sigma > 0 \in \mathbb{R}$, a scale parameter. Here σ affects the degree of smoothing in the image.

Due to the great success of linear scale space theory which includes a unifying view and robust implementations, provides a common way to think about local image geometry. The use of scale parameter detects essentially multi-local features in addition to local features. However, multi-local is not equivalent to multi-scale and the capturing of multi-local structure by enlarging scale in local operators is questionable. To avoid some or all of the three aforementioned problems, a large class of non-linear filters has been introduced. Mathematical morphology is truly non-linear one which works based on the morphological superposition principle. This does not signify that it is not connected with physical measurements. In fact, morphological dilation is used to describe the image formation process of the scanning probe microscope. The morphological operators carry local geometry in images from point to point, therefore mathematical morphology is closely connected with multi-local geometry.

2.1. Effects of the morphological operator

A very attractive property of mathematical morphology operators is its robustness under spatial variation, so-called *Lipschitz* transforms [42–45]. This mapping is a general one which includes projective transformation, rotation and translation, in addition to changes in viewpoint. Definitions and relation of *Lipschitz* operation or transform with mathematical morphology are described in Appendix A.

3. Proposed descriptor

Although the linear scale space approach to multi-scale image analysis has gained popularity due to its mathematical simplicity,

its close relation with Fourier analysis, and its plausibility for being used in earlier stages of the human vision system. However, linear scale space approach has some limitation as follows:

1. Linear filters can blur and shift the prominent features such as edges.
2. The use of parameter in linear scale space is not directly related with above mentioned size based definition of scale.
3. A compact shape representation of the signal can not be extracted by the multi-scale representation using linear filter.

Alternatively, a large class of non-linear filters have been introduced to overcome some or all of the three aforementioned problems. Mathematical morphology, which works based on the principle of morphological superposition, is truly non-linear one. Mathematical morphology is a useful tool for image analysis and it can directly measure the surface of an image. Through suppressing the details whose scale is less than that of the structuring element (SE), it provides us the ability to observe and measure the shape of an object at different scales. In order to reduce the time cost, this method uses only one variable SE which is able to characterize the spatial distribution of local image structure at multiple scales, to measure the image surface by iteratively dilate. The variable SE limits the improvement of the estimation accuracy, but benefiting from the ability of scale space analysis to distinguish spatial patterns.

3.1. Local morphology pattern

To construct the local morphology tower (Mt), we use the multi-scale morphology with a variable sized structure element (SE) as described by Maragos [41] followed by a smoothing pre-processing step (Fig. 3(a)). The isotropic Gaussian kernel G_σ (Eqn. (5)) of various sized are used for smoothing operation,

$$G_\sigma(x, y) = \frac{1}{\sigma\sqrt{2\pi}} \exp^{-\frac{(x^2+y^2)}{2\sigma^2}} \quad (5)$$

where we select the variance $\sigma = 0.5$ like scale invariant feature transform (SIFT) [46] and size of Gaussian kernels are same

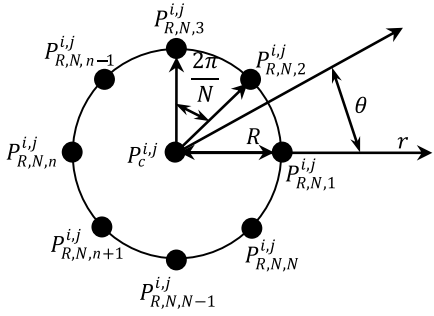


Fig. 4. The local neighbors $P_{R,N,n}^{i,j}$ for ($\forall n \in [1, N]$) of a center pixel $P_c^{i,j}$ in polar coordinate system.

as SEs. The multi-scale local MT is a stack of morphologically filtered representation of an image formed by multi-scale opening and closing using a family of convex and compact SEs, and its higher order homothetics. A MT resembles an image consisting of a stack of images with decreasing resolution and size of the image called morphological pyramid. In this work, MT stacks the morphological filtered images at increasing scale without changing the image resolution. Thus a MT corresponding to opening and closing of preprocessed images with a family of SEs (Fig. 3(a)) of sizes (3×3 , 5×5 , and 7×7) is formed by Eqn. (3). Here, MT which also satisfy the morphological scale space properties, is termed as local shape vector (Lsv). The Lsv for a given image I , $\bar{S} = (S_{(3 \times 3)}^o, S_{(3 \times 3)}^c, S_{(5 \times 5)}^o, S_{(5 \times 5)}^c, S_{(7 \times 7)}^o, S_{(7 \times 7)}^c)$ are represented as $\bar{S} = (S^1, S^2, \dots, S^{\alpha-1}, S^\alpha)$ where $\alpha \in [1, 2, \dots, 2 \times \#SE]$ and superscript ‘ o ’ and ‘ c ’ represent opening and closing with a different sized of convex SE. Fig. 3(b) shows an image MT obtained using the SE of varying sizes.

Finally, the local morphological pattern (LMP) for each element in the local shape vector (Lsv) for a given center pixel $P_c^{i,j}$ at (i, j) is computed by comparing its gray value $S_c^{i,j}$ with the gray value of a set of N local circularly and equally spaced neighbors $P_{R,N}^{i,j}$ with radius R around the center pixel $P_c^{i,j}$ (Fig. 4). LMP considers only those pixels as a center pixel whose all N local neighbors are within the image in scale space of dimension $M_x \times M_y$. In Fig. 4, the n th neighbor of $P_c^{i,j}$ (i.e. n th element of $P_{R,N}^{i,j}$) is denoted by $P_{R,N,n}^{i,j}$ having gray value $S_{R,N,n}^{i,j}$, where n is positive integer and $n \in [1, N]$. The spatial coordinate (x, y) of $P_{R,N,n}^{i,j}$ with respect to the origin of the image is given as

$$\begin{aligned} x(P_{R,N,n}^{i,j}) &= i + r(P_{R,N,n}^{i,j}) \times \cos(\theta(P_{R,N,n}^{i,j})) \\ y(P_{R,N,n}^{i,j}) &= j - r(P_{R,N,n}^{i,j}) \times \sin(\theta(P_{R,N,n}^{i,j})) \end{aligned} \quad (6)$$

where $i \in [R+1, M_x - R]$ and $j \in [R+1, M_y - R]$. $r(P_{R,N,n}^{i,j})$ and $\theta(P_{R,N,n}^{i,j})$ denote the polar coordinates of $P_{R,N,n}^{i,j}$ where $n = 1, 2, \dots, N$ and computed as

$$\begin{aligned} r(P_{R,N,n}^{i,j}) &= R \\ \theta(P_{R,N,n}^{i,j}) &= (n-1) \times \frac{2\pi}{N} \end{aligned} \quad (7)$$

Let $S_c^{i,j,l}$ be the center pixel (i, j) of l th element of shape vector ($l \in [1, \dots, \alpha]$) and $S_{R,N,n}^{i,j,l}$ is the n th neighbor of center $S_c^{i,j,l}$ corresponding to the equal spaced N sampling point around at radius R . The N binary values of LMP corresponding to the N neighbors of $S_c^{i,j,l}$ are represented as follows,

$$\bar{B}_{R,N}^{i,j,l} = [B_{R,N,1}^{i,j,l}, B_{R,N,2}^{i,j,l}, \dots, B_{R,N,n-1}^{i,j,l}, B_{R,N,N}^{i,j,l}] \quad (8)$$

where $B_{R,N,n}^{i,j,l}$ is a binary value in LMP corresponding to the n th neighbor of $S_c^{i,j,l}$ and computed as follows,

$$B_{R,N,n}^{i,j,l} = \text{sign}(\Delta_{R,N,n}^{i,j,l}) \quad (9)$$

where sign is a unit step function to find whether a given number is positive or not, and defined as follows,

$$\text{sign}(\theta) = \begin{cases} 1, & \text{if } \theta \geq 0 \\ 0, & \text{otherwise} \end{cases} \quad (10)$$

In Eqn. (9) $\Delta_{R,N,n}^{i,j,l}$ is the local morphological difference between a given center pixel $S_c^{i,j,l}$ and its n th neighbor $S_{R,N,n}^{i,j,l}$ for l th element of local shape vector (Lsv) and defined as

$$\Delta_{R,N,n}^{i,j,l} = S_{R,N,n}^{i,j,l} - S_c^{i,j,l} \quad (11)$$

We define the local morphological pattern (LMP) for a center pixel, $S_c^{i,j,l}$ corresponds to the l th element of Lsv using its local morphological sign difference defined in Eqn. (8) as follows,

$$\text{LMP}_{R,N}^{i,j,l} = \sum_{n=1}^N 2^{n-1} \times B_{R,N,n}^{i,j,l} \quad (12)$$

The values of the LMP depend on the number of neighbors (N) considered to form the pattern and which lies in between 0 to $2^N - 1$. We compute the local morphological patterns for all elements of Lsv. Fig. 3(b) shows the computed local morphological patterns ($\text{LMP}_{R,N}^{i,j,l}|l=1, 2, \dots, \alpha$) from each element of Lsv (morphology tower) for a texture image shown in Fig. 3(a).

3.2. LMP feature vector

To reduce the matching complexity of local morphological pattern (LMP), we need to compute the histogram, H of local morphological pattern (LMP) for each element of local shape vector (Lsv). The histogram of $\text{LMP}_{R,N}^{i,j,l}$, $H_{R,N}^l$ where $l \in [1, \alpha]$ is computed using the following equation,

$$H_{R,N}^l(\Omega) = \sum_{i=R+1}^{M_x-R} \sum_{j=R+1}^{M_y-R} \Psi(\text{LMP}_{R,N}^{i,j,l}(i, j), \Omega) \quad (13)$$

where $\Omega \in [0, 2^N - 1]$ and $\Psi(u, v)$ is a function given by

$$\Psi(u, v) = \begin{cases} 1, & \text{if } u == v \\ 0, & \text{otherwise} \end{cases}$$

The final LMP feature vector is constructed by concatenating all histograms $H_{R,N}^l$ where $l \in [1, \alpha]$. An important question is: should the histograms be normalized or not? Our experiments suggest that the LMP descriptor performed better using the histograms normalized, so that the contribution of each shape under different scale is proportion to the number of normalized patterns. In practice, the number of the structuring element is limited to 3. Since the number of bins in Eqn. (13) of $\text{LMP}_{R,N}^{i,j,l}$ for each element of Lsv ($l \in [1, \alpha]$) is 256 when $R = 1$, and $N = 8$, the dimension of the LMP feature vector for Lsv which contain six elements (six filtered images formed by morphological opening and closing operation with three sizes of SE) becomes $256 \times 6 = 1536$. In order to reduce the dimension of bins we adapt uniform pattern [27] selection scheme which generates 59 bins for each $\text{LMP}_{R,N}^{i,j,l}$ and the dimension of final normalized LMP feature vector is reduced to $59 \times 6 = 354$.

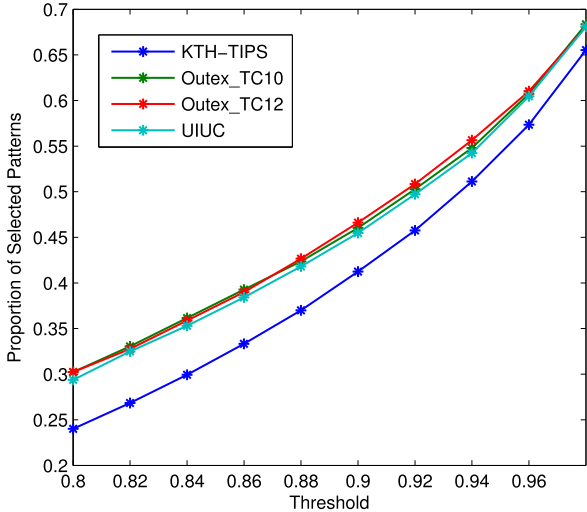


Fig. 5. Proportion of selected dominant feature vs threshold.

3.3. Feature selection

In this work, we also adopted a dominant feature selection technique [47] to learn the subset of discriminative pattern from the training images of each database. The most frequently occurring patterns in the training images are selected and used for classification. The most frequent patterns are found in the following way. First, final normalized LMP histogram denoted as H_1, H_2, \dots, H_N are computed for all training images. The pattern distribution of training images are found by summing up all the histograms bin-wise represented as $H = H_1 + H_2 + \dots + H_N$. The first K bins are selected from the summed histogram after sorting in the descending order. The value of K is calculated as follows,

$$K = \arg \min_K \frac{\sum_{i=1}^{K-1} H(i)}{\sum_{i=1}^L H(i)} > \lambda \quad (14)$$

where L is the dimension of final LMP descriptor and λ is the threshold parameter. Total number of selected bins (K) of the pattern by the above algorithm depends on the threshold parameter (λ) and training database. The effectiveness of the feature selection will be demonstrated in the experimental section. Fig. 5 shows the proportion of selected dominant patterns as the function of threshold (λ) for different texture suits (Outex_TC10, Outex_TC12, KTH-TIPS, and UIUC).

4. Feature distribution matching

The basic aim of feature similarity measurement is to calculate the distance between the feature vectors of test images and training model. After computing the LMP descriptors as described in the previous section, we need to represent their distributions in the training (model) and test images (sample). The dissimilarity of sample and model histograms is a test of goodness-of-fit, which can be measured with a non-parametric statistical test. There are many metrics for evaluating the fitness between two histograms, such as histogram intersection, log likelihood ratio, and chi-square (χ^2) kernel [27]. In this paper, the actual classification is performed via two non-parametric classifiers. First, the NNC with the chi-square (χ^2) distance is used to show the effectiveness of the proposed feature extraction scheme. To compare two histograms $H_1 = u_1, \dots, u_d$ and $H_2 = w_1, \dots, w_d$, we use the χ^2 distance defined as,

$$D(H_1, H_2) = \sum_{i=1}^d \frac{(u_i - w_i)^2}{u_i + w_i} \quad (15)$$

where d is the number of bins, H_1 and H_2 are the extracted features of a test sample and training sample. The class of test sample H_1 is assigned to the class of training sample H_2 that minimizes the χ^2 -distance.

Then another advanced classifier, called nearest regularized subspace (Nrs) classifier [49], is implemented to further improve the classification performance. In multi-class classification, a given test sample $y \in \mathbb{R}^d$ is to be assigned to one of the L classes. Let us consider x_i is the i th training sample and all training samples are stacked into a matrix $\mathbf{X} = \{x_i\}_{i=1}^n \in \mathbb{R}^{d \times n}$ and labels of classes are $\omega_i \in \{1, 2, \dots, L\}$, where L and n represent the number of classes and total number of training samples. Assume n_l is the number of available training samples for the l th class, where $\sum_{l=1}^L n_l = n$. A class specific approximation of test sample y is calculated based on a linear combination of available training samples per class. If \mathbf{X}_l is the total training samples of l th class, then \bar{y}_l , the class specific approximation of test sample y is calculated as follows

$$\bar{y}_l = \mathbf{X}_l \alpha_l \quad (16)$$

where \mathbf{X}_l is of size $d \times n_l$ and α_l is a $n_l \times 1$ vector of weighted coefficients. The class of test sample y is assigned to those labeled of class for which the residual is minimized, i.e.,

$$\text{class}(y) = \arg \min_{l=1, \dots, L} (r_l) \quad (17)$$

where $r_l = \|\bar{y}_l - y\|_2$ represents residual between the class specific approximation and corresponding test sample to be classified.

In Nrs [49], α_l represents class specific weight vector and calculated as follows

$$\alpha_l = \arg \min_{\alpha^*} \|y - \mathbf{X}_l \alpha^*\|_2 + \tau \|\Gamma_{l,y} \alpha^*\|_2 \quad (18)$$

where $\Gamma_{l,y}$ represents biasing Tikhonov matrix [50] corresponding to l th class and test sample y to be classified, τ is a global regularization parameter (best result achieve when $\tau = 5 \times 10^{-2}$) which balances the minimization between the residual and regularization terms, and α^* is different value of α_l . Mathematically, a diagonal representation of $\Gamma_{l,y}$ is in the following form

$$\Gamma_{l,y} = \begin{bmatrix} \|y - x_{l,1}\|_2 & 0 \\ & \ddots \\ 0 & \|y - x_{l,n_l}\|_2 \end{bmatrix}$$

where $x_{l,1}, x_{l,2}, \dots, x_{l,n_l}$ are the elements of columns of matrix \mathbf{X}_l for the l th class. According to Eqn. (18), the class specific weight vector α_l is calculated as follows

$$\alpha_l = (\mathbf{X}_l^T \mathbf{X}_l + \tau^2 \Gamma_{l,y}^T \Gamma_{l,y})^{-1} \mathbf{X}_l^T y \quad (19)$$

5. Experimental results

To evaluate the effectiveness of the proposed descriptor, we carried out a series of experiments on five well known large and commonly used texture databases KTH-TIPS [37], UIUC [38], Outex_TC-00010 (Outex_TC10) [4], and Outex_TC-00012 (Outex_TC12) [4]. The sample images from KTH-TIPS, UIUC, Outex_TC10 texture databases are shown in Figs. 6, 8 and 9. A detailed description of these databases are summarized in Table 1.

There are 24 different homogeneous texture classes selected from the Outex texture databases [4], with each having the images of size 128×128 pixels. Outex_TC_00010 (**Outex_TC10**) contains texture images under illuminant “inca” and 0° an-

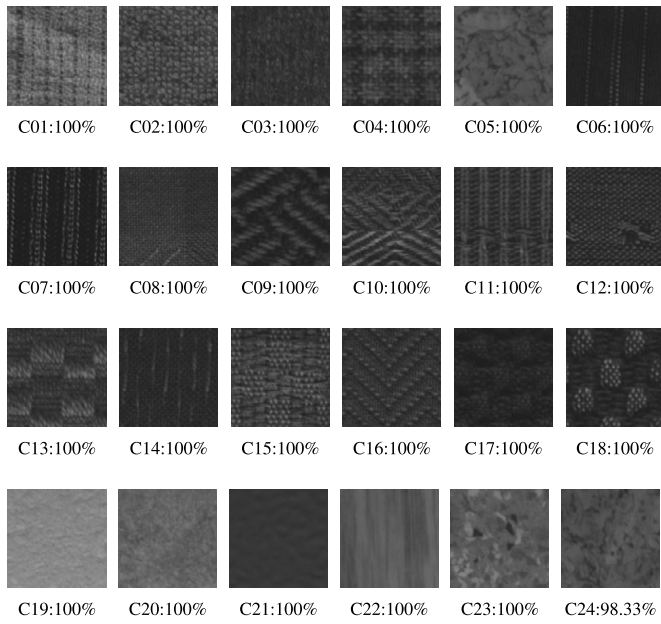


Fig. 6. The per-class average classification accuracy (%) achieved by proposed descriptor with Nrs classifier on Outex_TC10 [4] texture database.

gel in each texture class. Outex_TC_00012 (**Outex_TC12**) texture images of each class are collected under 3 different lighting conditions (“inca”, “horizon”, and “t184”) and 9 different rotation angles ($0^\circ, 5^\circ, 10^\circ, 15^\circ, 60^\circ, 75^\circ$, and 90°). Two experiment test suites Outex_TC_00010 (**Outex_TC10**), and Outex_TC_00012 (**Outex_TC12**) are summarized in Table 1.

The KTH-TIPS [37] database contains texture images with 3 different viewing angles, 4 illuminants, and 9 different scales and have the dimension of 200×200 , as depicted in Table 1. The samples of ten images are shown in Fig. 8.

The UIUC [38] database contains 40 images in each of 25 different texture classes, thereby making 1000 images of resolution 640×480 . The database represents a major improvement over the CUReT textures [51] where the materials are captured under significant viewpoint variations and some have considered under surface deformation and are summarized in Table 1. However, a drawback is that the number of sample images per class is much smaller than those in the CUReT database. It also has very few examples of a given material so it is difficult to perform classification experiments [52]. In addition, high resolution of the images makes it unclear how features will perform in a real world setting where textured regions for an object may be much smaller. In spite of these, as far as viewpoint and scale variations are concerned, the UIUC is one of the most challenging texture database.

The performance of proposed LMP descriptors is evaluated in term of classification accuracy with K-fold cross-validation test using two non-parametric classifiers, namely nearest neighbor classifier (NNC) with chi-square (χ^2) distance and nearest regularized subspace (Nrs) classifier where $K = 10$ is chosen empirically. In K-fold cross-validation test, the feature set is randomly sorted and divided into K equal size subset. In each round of validation one feature subset is used for testing the model and, remaining $K - 1$ feature subsets are used as training data. The validation process is repeated K times (the folds) where each of K subsets used once as the validation data. The average of classification accuracies over K rounds is used to obtain final cross-validation accuracy. The K -fold cross-validation process provides a more accurate and reliable picture of the classification model. The performance of the proposed descriptor is compared with $LBP_{R,N}$ [27], $LBP_{R,N}^{u2}$, $DLBP_{R,N}$ [29],

Table 1
Details of four texture datasets.

Description	Texture databases			
	KTH-TIPS	UIUC	Outex_TC10	Outex_TC12
Total class	10	25	24	24
Number of images	81	40	180	200
Resolution	200×200	640×480	128×128	128×128
Scale variation	✓	✓	✓	✓
Illumination		✓	✓	✓
Rotation	✓	✓	✓	✓

$LBP_{R,N}^{sri_su2}$ [36], multiscale $CLBP_S_{R,N}^{riu2}/M_{R,N}^{riu2}/C(1, 8 + 3, 16 + 5, 24)$ [5] and some other state-of-the-art methods.

In this section, performance of the proposed LMP descriptor is evaluated by applying it to texture classification task. The parameters for the proposed descriptor are set as the same through all the experiments. The scale range of the structuring elements (SEs) which are used for estimating the morphological “opening” and “closing”, set to be a series of integers 3×3 , 5×5 , and 7×7 . The encoding of morphological scale space of a texture image is done using uniform local morphological pattern ($LMP_{R,N}^{u2}$) where (R, N) set as $R = 1$ and $N = 8$.

5.1. Experiment on Outex database

The results of the experiment carried out on two Outex databases, Outex_TC10 and Outex_TC12 are tabulated in Table 2. This table includes the average classification accuracy of K -fold ($K = 10$) cross validation test for the proposed descriptor and recent state-of-the-art methods. According to the results of Table 2, we could make the following observations.

$CLBP_S/M/C$ achieves highest performance compared to other variant of $CLBP$. This is because it is made by fusing $CLBP_S$ and $CLBP_M/C$ and contains complementary features of sign and magnitude, in addition the center pixel information which represents the grey level of the local structure. LTP provides the worse performance compared to other LBP methods because it quantizes the local difference into three levels and another reason is that LTP is decomposed into one negative and one positive LBPs, which are not independent to each other.

Since contrast is measured locally, the pattern of a texture and contrast are complementary features, so it can be expected to get good classification performance using both rather than using one alone. The LBP/VAR provides good classification performance compared to $LBPV$, because the useful information is lost in the integral projection. Sometimes $LBPV$ may provide better result using a suitable global matching scheme with larger scale. However, it increases feature dimensionality significantly [30].

$DLBP$ gives improved performance compared to original LBP because it uses only the most frequently occurred patterns of LBP (around 80%). However, like VAR it neglects the local spatial structure which carries important information for texture discrimination. In addition $DLBP$ approach needs a pretraining stage and its dimensions varies with the training samples.

$VZ-MR8$ and $VZ-Patch$, are popular examples of statistical algorithm and takes dense response from multiple filter. However, the performance of $VZ-MR8$ and $VZ-Patch$ are significantly lesser compared to proposed LMP descriptor. While the cost of feature extraction and matching is quite high. Both of them extract eight maximum filter response from 38 filtered images and then textron histogram is built by clustering technique.

$LBP_{R,N}^{NT}$ and $BRINT$ provide quite impressive classification performance compared to other LBP methods, but lower than proposed LMP descriptor. $LBP_{R,N}^{NT}$ includes feature extraction using locally rotation invariant approach which creates 10 bins that may be unable to represent each class well and $BRINT$ include multi-

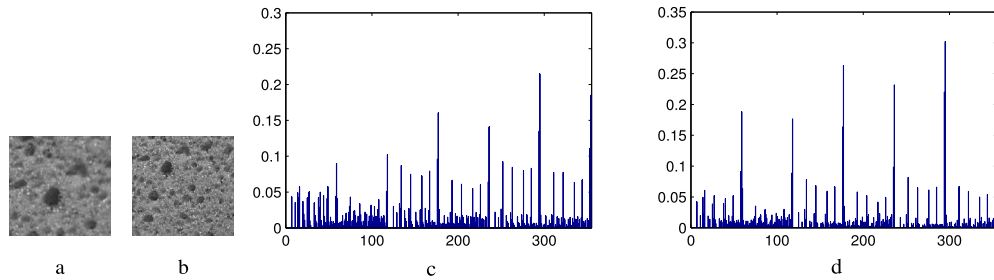


Fig. 7. Example to illustrate scale effectiveness of the proposed descriptor.

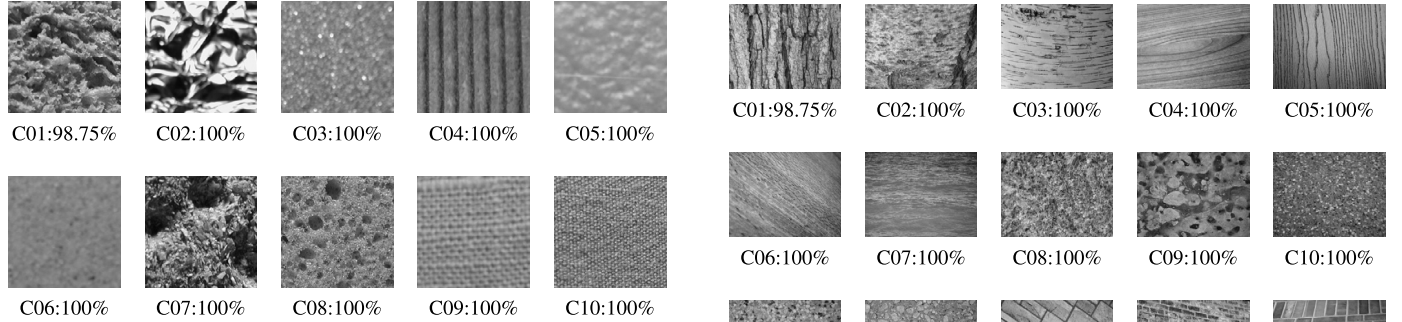


Fig. 8. The per-class average classification accuracy (%) achieved by proposed descriptor with Nrs classifier on KTH-TIPS [37] database.

resolution ($R = 1, 2, \dots, 4$) feature extraction, by utilizing rotation invariant LBP approach while it may lose global image information when only the local rotation invariant features are used.

The proposed LMP descriptor provides superior classification performance compared to other state-of-the-art methods in term of mean accuracy and standard deviations i.e. $99.88 \pm 0.1618\%$, $99.79 \pm 0.1851\%$, and $99.76 \pm 0.1952\%$ for Outex_TC10, Outex_TC12 (“horizon”, and “t184”), respectively, using NNC classifier. The performance of the proposed descriptor is further improved when an advanced non-parametric Nrs classifier is used and class-wise accuracy is shown in Fig. 6. The proposed LMP descriptor is obtained from the morphological scale space representation of a texture image which is formed using non-linear morphological operations and avoids the problems of linear scale space representation. It achieves reasonable performance due to the following characteristic. The multi-scale opening creates flat regions by removing bright objects or its parts smaller than the SE. The properties $f \circ \psi \leq f$ and $f \circ {}^i\psi \geq f \circ {}^j\psi$ for $i < j$ indicate that no new regional maxima is generated at higher scales due to the opening. Similarly, in case of multi-scale closing, no new regional minima is generated at higher scales. Morphological operations leaves the image details whose scale is larger than the SE. Furthermore, it is shown that multi-scale local morphological operation, “opening” and “closing” are invariant to Lipschitz transforms, whereas its extension is able to correctly discriminate between the fundamental texture primitives. The successive responses of opening and closing by a scalable SE together known as local shape vector (Lsv) in the morphology scale space representation. The proposed pattern is built from each element of Lsv which preserves micro as well as macro shape of texture image. The final feature vector achieves scale invariance by taking joint distribution of all the histograms of LMP.

5.2. Experiments on KTH-TIPS & UIUC database

To analysis the scale invariance property of the proposed descriptor, the experiment is carried out on KTH-TIPS benchmark database which contains texture images with different scale variations. Fig. 7 shows a sample texture image to demonstrate

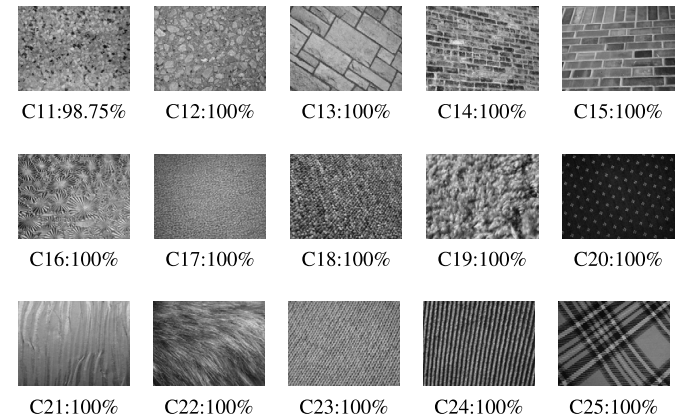


Fig. 9. The per-class average classification accuracy (%) achieved by proposed LMP descriptor with Nrs classifier on UIUC [51] texture database.

Table 2

Average classification accuracy (%) of proposed and STATE-OF-THE-ART schemes on Outex_TC10 and Outex_TC12.

Method	Classifier	Outex_TC10		Average
		Outex_TC10 horizon	Outex_TC10 t184	
LTP [32]	NNC	76.06	63.42	62.56
VAR [26]	NNC	90.00	64.35	62.93
LBP [27]	SVM	97.60	85.30	91.30
LBP ^{iu2} _{R,N}	NNC	84.89	63.75	65.30
LBP/VAR	NNC	96.56	78.08	79.31
LBPV ^{iu2} _{R,N} [30]	NNC	91.56	77.01	76.62
CLBP_S	NNC	84.81	63.68	65.46
CLBP_M	NNC	81.74	62.77	59.30
CLBP_M/C	NNC	90.36	76.66	72.38
CLBP_S/M/C [5]	NNC	94.53	82.52	81.87
CLBP_S/M	NNC	94.66	83.14	82.75
CLBP_S/M/C	NNC	98.93	92.29	90.30
LBP ^N _{R,N} [54]	NNC	99.24	96.18	94.28
DLBP _{R=3,N=24} [29]	SVM	98.10	87.40	91.60
BINT_Cs_CM [55]	NNC	99.35	97.69	98.56
VZ-MR8 [56]	Nsc	93.59	92.82	92.55
VZ-Patch [57]	Nsc	92.00	92.06	91.41
Ptp [58]	NNC	99.56	98.08	97.94
CDCP [53]	NNC	99.76	99.82	99.62
Proposed LMP	NNC	99.88	99.79	99.76
Proposed LMP	Nrs	100.0	99.95	99.97
				99.81

Table 3

Comparing the average classification accuracy achieved by the proposed approach with those achieved by recent state-of-the-art methods.

Methods	Classifier	Classification accuracy (%)	
		KTH-TIPS [37]	UIUC [38]
VZ-MR8 [56]	NNC	94.50	–
VZ-Patch [57]	NNC	92.40	97.83
Lazebnik et al. [38]	NNC	91.30	96.03
Zhang et al. [20]	SVM	96.10	98.70
BIF [25]	Shift NNC	98.50	98.80
MFS [59]	NNC	81.62	92.74
PLS [6]	SVM	97.35	96.57
BRINT [55]	NNC	97.75	–
LBP _{1,8} ^{riu2} [27]	NNC	82.67	55.26
DLBP _{3,24} [29]	SVM	86.99	60.73
LBP _{1,8} ^{sri-su2} [36]	NNC	89.73	70.05
LBP _(1,8+2,16+3,24) [27]	NNC	95.17	76.88
CLBP_SMC [5]	NNC	97.19	93.26
Varma and Garg [17]	NNC	–	95.40
SSLBP [60]	NNC	97.80	97.02
LDZP [48]	NNC	97.82	–
Proposed LMP	NNC	98.37	97.12
Proposed LMP	NRS	99.87	99.90

the effectiveness of scale invariance of the proposed descriptor. Fig. 7(a)–(b) shows texture images of same material from KTH-TIPS database with different scales (1 & 3) and Fig. 7(c)–(d) shows the histogram of proposed LMP for scale 1 and scale 3 images. It is observed from the demonstration in Fig. 7 that the joint distribution of the proposed descriptors for intra-class images with sufficiently different scales are approximately close. The experiments are repeated 10 times with randomly chosen training samples and the average accuracies are reported in Table 3. The proposed descriptor achieves classification performance in term of mean accuracy and its standard deviation, $98.50 \pm 0.7905\%$ and $99.87 \pm 0.8436\%$ using NNC and NRS classifiers, respectively.

The performance of the proposed descriptor is also evaluated on more challenging UIUC database, which contains high resolution texture images in addition to scale and viewpoint variations. The high resolution does not provide clear information how the texture feature will perform in a real world scenario where texture regions on objects may be much smaller.

The comparative performance of the proposed descriptor with other state-of-the-art methods are summarized in Table 3. It is observed that the performance of the proposed descriptor is much better than recent state-of-the-art statistical methods i.e., VZ-MR8 and VZ-Patch. SSLBP method provides good classification performance compared to popular CLBP and other variant of LBP but lesser than LMP descriptor. This is because SSLBP which formed the scale space representations of texture image by convolving 2-D Gaussian filter with different scales, selects the maximum frequency from CLBP patterns. However, SSLBP does not establish any relationship between scales and images. The propose descriptor using NNC gives comparable performance as compared to the BIF [25] at multiple scales, $\sigma, 2\sigma, 4\sigma$ and 8σ . Although BIF provides good classification performance, but it uses pyramid histogram with computationally inefficient shift matching NNC. In addition the feature dimension of BIF is too large. Although the images of UIUC are captured by varying scale and different view-point, the proposed descriptor achieves the classification performance in term of mean accuracy and standard deviations, $97.12 \pm 0.3587\%$ and $99.90 \pm 0.2850\%$ using NNC and NRS classifier, respectively. It is observed that the proposed descriptor outperforms recent state-of-the-art methods.

Though the trend is clear from the performance Table 2 and 3, we have further analyzed the performance using one way statistical analysis of variance (ANOVA) test [61]. ANOVA is a collection of statistical test used to analyze the differences among group

Table 4

One way statistical ANOVA test result for Outex_TC10 & Outex_TC12 (horizon and t184), KTH-TIPS and UIUC texture databases, where level of significance selected as $\alpha = 0.05$.

Source	SS	df	MS	F	Prob (p) > F
Groups	2990.45	06	498.408	8.32	0.000043
Error	1557.05	26	59.887		
Total	4547.50	32			

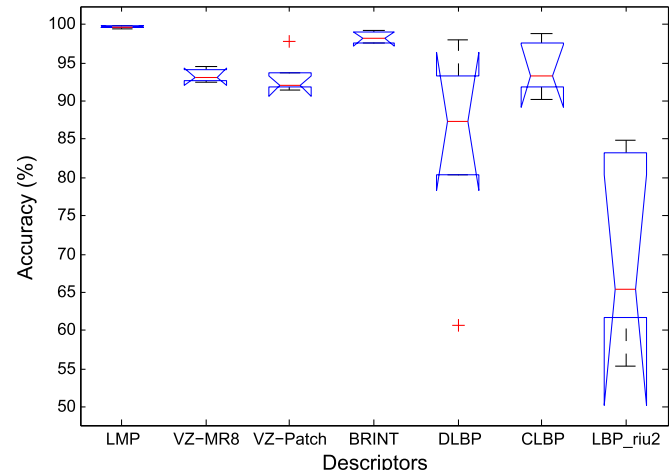


Fig. 10. The box plot (descriptor vs. accuracy) corresponding to one way statistical ANOVA test for proposed LMP and other state-of-the-art methods on Outex_TC10 & Outex_TC12 (horizon and t184), KTH-TIPS and UIUC texture databases.

means and their associated procedures. The null hypothesis H_0 for the test indicates that, *there is no significant difference among group means*. We can reject H_0 if the p -value for an experiment is less than the selected significant level and which implies that at least one group mean is significantly different from the others. To understand the performance of the proposed descriptor LMP was significantly differs than well-known descriptors such as LBP_{1,8}^{riu2}, CLBP_S/M/C, DLBP, BRINT, VZ-Patch, and VZ-MR8, we conduct an one way ANOVA test with significance level is kept as $\alpha = 0.05$ and the test results are shown in Table 4. It is observed from Table 4 the p -value (0.000043) is less than the selected significant level $\alpha = 0.05$ and this indicates the performance of the proposed descriptor significantly differs from other descriptors and hence reject the hypothesis H_0 . In addition, the box plot corresponding to aforementioned ANOVA test is shown in Fig. 10, which clearly indicates the mean performance of the proposed descriptor is significantly better than the well-known descriptors such as LBP_{1,8}^{riu2} [27], CLBP_S/M/C [5], DLBP [29], BRINT [55], VZ-Patch [57], and VZ-MR8 [56]. To quantify the Gaussian distribution of the performance results using the proposed LMP and other well-known descriptors such as LBP_{1,8}^{riu2}, CLBP_S/M/C, DLBP, VZ-Patch, we conduct an one-sample Kolmogorov-Smirnov test (KS test) [62]. The test returned the value of $h = 1$ which indicates that KS test rejects the null hypothesis at the default 5% significance level.

To observe the individual performance of the proposed LMP descriptors created by different morphological operations with different size of SES, the experiment are separately conducted on Outex_TC10 & Outex_TC12 (horizon and t184), KTH-TIPS and UIUC texture databases and the performances are tabulated in Table 5. The comparative results of Table 5 shows that LMP for difference size of SES created by Opening–Closing operation provides better texture classification performance compared to LMPs created by individual Opening and Closing operations and the classification performances proportionally reduce with increasing size of SES. Table 5 also shows that combined LMP created from multi-

Table 5

The average texture classification accuracy (%) of the proposed descriptor created by different morphological operations with three different size of SES on Outex_TC10 & Outex_TC12 (horizon and t184), KTH-TIPS and UIUC texture databases.

Databases	Classifier	Opening				Closing				Opening–closing			
		3 × 3	5 × 5	7 × 7	Combined	3 × 3	5 × 5	7 × 7	Combined	3 × 3	5 × 5	7 × 7	Combined
Outex_TC10	NNC	99.35	97.89	93.72	99.25	99.69	99.23	97.31	99.72	99.79	99.69	98.70	99.88
	NRS	99.74	99.09	96.15	99.93	99.90	99.51	98.10	99.95	99.97	99.97	99.46	100.0
Outex_TC12 (horizon)	NNC	99.53	98.21	94.53	99.23	99.58	99.25	97.80	99.72	99.74	99.56	99.00	99.79
	NRS	99.74	98.86	96.73	99.95	99.90	99.51	98.84	99.93	99.97	99.93	99.88	99.95
Outex_TC12 (t184)	NNC	99.16	97.91	93.84	99.23	99.30	99.05	97.45	99.53	99.53	99.56	98.93	99.76
	NRS	99.58	98.75	96.71	99.90	99.81	99.60	98.56	99.90	99.95	99.83	99.69	99.97
KTH-TIPS	NNC	94.32	92.62	91.37	97.37	96.12	94.50	90.00	98.12	97.12	97.62	97.37	98.37
	NRS	96.50	93.50	91.63	97.75	98.87	95.37	91.25	98.87	99.25	98.25	97.50	99.87
UIUC	NNC	76.42	76.65	74.82	81.67	81.27	79.45	75.05	83.02	83.65	84.55	83.40	97.12
	NRS	88.02	84.37	80.85	92.57	91.97	88.35	83.10	94.42	94.80	93.45	92.25	99.90

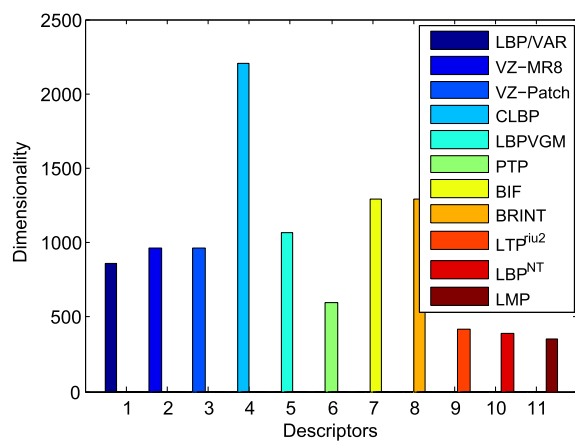


Fig. 11. Comparison of feature dimensionality between proposed and other state-of-the-art feature.

ple scale (multiple sizes of SES) provides better texture classification performance compared to individual scale and highest one is provided by combined Opening–Closing. The dimensionality of the proposed descriptors and other state-of-the-art methods are shown in Fig. 11. This figure clearly indicates that the dimensionality of the proposed descriptor (LMP has dimensionality 354) is significantly less compared to other state-of-the-art methods.

5.3. Comparison of Proposed LMP with state-of-art deep learning based methods

A key characteristic of deep convolution neural networks (CNN) (see Fig. 12) is a hierarchical representation which is universal and directly generated from data, used to perform image classification task. Deep CNNs have shown their power for recognition as a universal representation. However, robustness for recognition have been limited due to the lack of geometric invariance of global CNN activations. An effective texture descriptor FV-CNN has been introduced by Cimpoi et al. [9], where first CNN features are extracted at multiple scale levels then an order-less Fisher Vector pooling

Table 6
The texture classification performance and feature dimensionality of the proposed LMP and state-of-art deep learning based methods.

Methods	Classification accuracy (%)				Feature dimension	
	Outex_TC10	Outex_TC12	KTH-TIPS	UIUC		
FV-VGGDM (Svm) [8,9]	80.00	82.30	88.20	99.80	65536	
FV-AlexNet (Svm) [7,8]	67.30	72.30	77.90	99.10	32768	
ScatNet (Pca) [63,64]	99.69	99.06	68.92	96.15	596	
ScatNet (NNC) [63,64]	98.59	98.10	63.66	88.64	596	
PCANet (NNC) [12]	39.87	45.53	59.43	57.70	2048	
PCANet ^{iu2} (NNC) [12]	35.36	40.88	52.15	49.80	80	
RandNet (NNC) [12]	47.43	52.45	60.67	56.57	2048	
RandNet ^{iu2} (NNC) [12]	43.54	45.70	56.90	48.20	80	
Proposed LMP (NNC)	99.88	99.77	98.37	97.12	354	
Proposed LMP (NRS)	100.0	99.96	99.87	99.90	354	

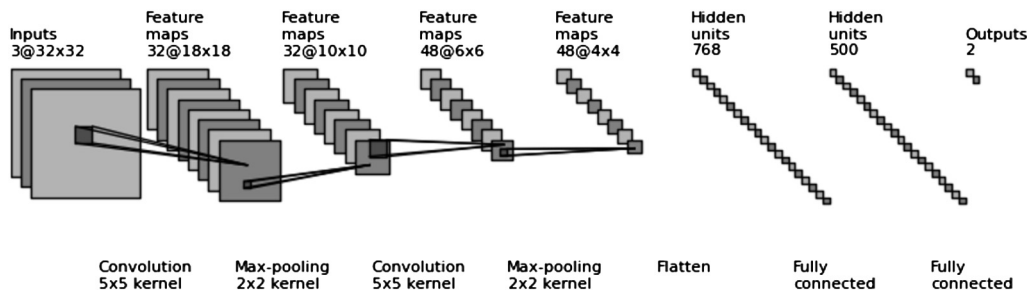


Fig. 12. A Deep Convolutional Neural Network architecture where the input is processed in a feed forward manner through the stage of convolutions and sub-sampling and finally classified with a linear classifier.

Table 7

Average feature extraction time using proposed LMP and matching time with NNC & NRS classifiers.

Feature extraction time (sec)	Texture databases			
	KTH-TIPS	UIUC	Outex_TC10	Outex_TC12
Proposed LMP	0.19	0.36	0.12	0.10
Matching NNC	0.012	0.017	0.093	0.116
Matching NRS	0.053	0.127	0.418	0.423

operation is performed. Despite the significant progress of deep CNN models, still there are little insight into the internal operation and behavior. Mallat et al. [63,64] have been introduced the scale and rotation invariant wavelet convolution scattering network (ScatNet) where the convolution filters are pre-defined as wavelet and no learning process is needed. Inspired by ScatNet, a simple deep learning network, PCANET is proposed by Chan et al. [12] which is based on cascading of multistage principal component analysis (PCA), binary hashing and histogram pooling. A simple variation of PCANET, RandNet [12], in which the cascaded filters are randomly selected but not learned also introduced by Chan et al. One of the major trends in deep CNN research community is to use more and more complex networks to improve the classification performances. However, it needs the powerful and large memory computer and GPUs to train very deep and computationally expensive networks. The comparative result of texture classification performance with feature dimensionality of the proposed LMP and state-of-art deep learning based methods such as FV-CNN [8,9], ScatNet [63,64], PCANet, PCANet^{riu2}, and RandNet [12], are tabulated in Table 6. It is observed from Table 6 that the proposed LMP provide comparable or better classification performance compared to state-of-art deep learning based methods. In addition the feature dimension of proposed LMP descriptor is also less than the deep learning based models.¹

We have implemented the algorithm in MATLAB 2011 environment and executed the program on Intel® Core™2 Duo CPU T6400 @ 2.00 GHz × 2 processor and 3 GB RAM with UBUNTU 14.04 LTS operating system. Table 7 listed the average feature extraction and matching time cost per-image on four benchmark texture database by the proposed LMP descriptor. It has been observed that the complexity of the proposed LMP descriptor linearly varies with the image size and the matching complexity also varies linearly with the number of training samples. It shows that the proposed descriptor is fast enough for real time applications.

6. Conclusion

This paper proposes a new and novel Local Morphology Pattern (LMP) descriptor for texture classification. Here first, a morphological scale space is built using morphological operations with different sized structuring elements (SEs). Then LMP is computed by encoding the relation between center and its neighboring pixels for all scale space representation of a texture image so-called local shape vector (Lsv) where the sharp and perfectly localized contours of the objects are well preserved even though the details vanish from one scale to another. To achieve scale invariance, the normalized histogram of LMP is established by joint distribution of histogram of LMP for all elements of Lsv. It is shown that LMP is invariant under local Lipschitz transform and its extension is adequate to correctly differentiate between the fundamental texture primitives. It is worth noting that the LMP is simple and very efficient to compute. Therefore an image with high resolution does not demand expansive computational burden by LMP descriptor. Extensive experiments are carried out on three benchmark texture

databases that include scale and rotation with illumination variations. The experimental results demonstrate that the proposed LMP descriptor outperforms a variant of LBP based descriptor as well as other state-of-the-art methods for texture classification task.

Acknowledgments

The authors sincerely thank Machine Vision Group (MVG), University of Oulu, Finland, Visual Geometry Group (VGG), University of Oxford, UK, and Department of Computer Science, University College London, UK for sharing the source codes of LBP, VZ-MR8 and BiF.

Appendix A. Lipschitz and mathematical morphology

Definition A.1. Lipschitz function: A function $f: \mathbb{R}^2 \rightarrow \mathbb{R}^2$ is called a member of the class of Lipschitz functions \mathcal{L} , if there exists a finite real value k such that $\forall x \neq y$,

$$\frac{|f(x) - f(y)|}{\|x - y\|} \leq k \quad (\text{A.1})$$

where $\|x - y\|$ represents the Euclidean distance between point x and y . The Lipschitz condition has a relationship with mathematical morphology through the elementary-shaped structure function.

Definition A.2. Elementary structure function: The elementary shaped structure function ${}^\rho\psi(x)$ with parameter of width ρ is defined as ${}^\rho\psi(x) = -\rho\|x\|$.

The elementary structure function has a few straightforward properties as follows,

- The dilation of two elementary structures is equal to the larger of two i.e. ${}^\rho\psi \oplus {}^\mu\psi = {}^{\rho \cap \mu}\psi$. Closing an arbitrary function f with a structure element is equal to the dilation of f with the structure element i.e. $f \bullet {}^\rho\psi = f \oplus {}^\rho\psi$. Opening an arbitrary function f with a structure element is equal to the erosion of f with the structure element i.e. $f \circ {}^\rho\psi = f \ominus {}^\rho\psi$. To define a precise definition of the Lipschitz condition, we distinguish between upper semi-Lipschitz (u.s.l.) function and lower semi-Lipschitz (l.s.l.) function as follows,

Definition A.3. Semi-Lipschitz: a function $f: \mathbb{R}^2 \rightarrow \mathbb{R}^2$ is called a member of the class of lower semi-Lipschitz functions if $\exists \rho \in \mathbb{R}^+: f = f \ominus {}^\rho\psi$. Similarly, a function $f: \mathbb{R}^2 \rightarrow \mathbb{R}^2$ is called a member of the class of upper semi-Lipschitz functions if $\exists \rho \in \mathbb{R}^+: f = f \oplus {}^\rho\psi$.

Theorem 1. A function $f: \mathbb{R}^2 \rightarrow \mathbb{R}^2$ is Lipschitz iff it is both lower semi-Lipschitz and upper semi-Lipschitz.

Proof. If f is upper semi-Lipschitz then,

$$\exists \rho : f = f \oplus {}^\rho\psi = f \quad (\text{A.2})$$

Let k^+ be that value of ρ , so we can write:

$$\forall x : f(x) = \vee_y [f(y) - k^+ \|x - y\|] \quad (\text{A.3})$$

or equivalently,

$$\forall x, y : f(x) \geq f(y) - k^+ \|x - y\| \quad (\text{A.4})$$

or

$$\forall x, y : \frac{f(x) - f(y)}{\|x - y\|} \geq -k^+ \quad (\text{A.5})$$

¹ The results of deep learning based methods are taken from Liu et al. [11].

Because f is also lower semi-Lipschitz: so we also have:

$$\exists \rho : f \ominus {}^\rho \psi = f \quad (\text{A.6})$$

Let k^- be that value of ρ , so we can write:

$$\forall x, y : f(x) \leq f(y) + k^- \|x - y\| \quad (\text{A.7})$$

or

$$\forall x, y : \frac{f(x) - f(y)}{\|x - y\|} \leq k^- \quad (\text{A.8})$$

Using $k = k^+ \cup k^-$ and combining Eqn. (A.5) and (A.8) we obtain:

$$\forall x, y : \frac{f(x) - f(y)}{\|x - y\|} \leq k \quad (\text{A.9})$$

This is obviously equivalent with the Lipschitz condition of the Definition A.1. \square

Every Lipschitz function $f : \mathbb{R}^2 \rightarrow \mathbb{R}^2$ is characterized with two scalar values are as follows,

$$\begin{aligned} f_L^+ &= \min\{\rho | f \oplus {}^\rho \psi = f\} \\ f_L^- &= \min\{\rho | f \ominus {}^\rho \psi = f\} \end{aligned} \quad (\text{A.10})$$

The importance of Lipschitz functions in mathematical morphology [43] is that the class of Lipschitz functions is closed under dilations and erosions irrespective of the structuring function is used.

Proposition 1. Let $f \in \mathcal{L}$ then for any structuring function g , $f \oplus g \in \mathcal{L}$ and $f \ominus g \in \mathcal{L}$.

Proof. Here we provide the proof of erosion. Of course if f is Lipschitz then $-f$ is also Lipschitz. Thus the duality used to satisfy $f \oplus g \in \mathcal{L}$ if we show $f \ominus g \in \mathcal{L}$. For the erosion we have:

$$(f \ominus g) \ominus {}^\rho \psi = (f \ominus {}^\rho \psi) \ominus g$$

Since $f \in \mathcal{L}$ so we have

$$\rho \geq f_L^- : f \ominus {}^\rho \psi = f$$

and thus,

$$\rho \geq f_L^- : (f \ominus g) \ominus {}^\rho \psi = (f \ominus {}^\rho \psi) \ominus g = f \ominus g \quad (\text{A.11})$$

showing that $f \ominus g$ is lower semi-Lipschitz. For dilation $(f \ominus g) \oplus {}^\rho \psi$ can be written as

$$(f \ominus g) \oplus {}^\rho \psi = (f \ominus g) \bullet {}^\rho \psi \geq f \ominus g \quad (\text{A.12})$$

We know that in general $(f \ominus g) \oplus h \leq (f \oplus h) \ominus g$. This implies that

$$(f \ominus g) \oplus {}^\rho \psi \leq (f \oplus {}^\rho \psi) \ominus g$$

Since f is Lipschitz, therefore $\rho \geq f_L^+ : f \oplus {}^\rho \psi = f$ and thus $\rho \geq f_L^+ : (f \ominus g) \oplus {}^\rho \psi \leq f \ominus g$. Combined with Eqn. (A.12) we can write

$$\rho \geq f_L^+ : (f \ominus g) \oplus {}^\rho \psi = f \ominus g. \quad (\text{A.13})$$

From Eqn. (A.11) and Eqn. (A.13) we write,

$$\rho \geq (f_L^- \vee f_L^+) : (f \ominus {}^\rho \psi) \ominus g = (f \ominus g) \oplus {}^\rho \psi = f \ominus g$$

showing that $f \ominus g$ is Lipschitz. \square

References

- [1] X. Xie, M. Mirmehd, A galaxy of texture features, in: *Handbook of Texture Analysis*, World Scientific, 2008, pp. 375–406.
- [2] M. Tuceryan, A.K. Jain, et al., Texture analysis, in: *Handbook of Pattern Recognition and Computer Vision*, vol. 2, 1993, pp. 207–248.
- [3] S. Umer, B.C. Dhara, B. Chanda, A novel cancelable iris recognition system based on feature learning techniques, *Inf. Sci.* 406 (2017) 102–118.
- [4] T. Ojala, T. Maenpaa, M. Pietikainen, J. Viertola, J. Kyllonen, S. Huovinen, Outex – new framework for empirical evaluation of texture analysis algorithms, in: *Pattern Recognition, 2002. Proceedings. 16th International Conference on*, Vol. 1, IEEE, 2002, pp. 701–706.
- [5] Z. Guo, L. Zhang, D. Zhang, A completed modeling of local binary pattern operator for texture classification, *IEEE Trans. Image Process.* 19 (6) (2010) 1657–1663.
- [6] Y. Quan, Y. Xu, Y. Sun, A distinct and compact texture descriptor, *Image Vis. Comput.* 32 (4) (2014) 250–259.
- [7] A. Krizhevsky, I. Sutskever, G.E. Hinton, ImageNet classification with deep convolutional neural networks, in: *Advances in Neural Information Processing Systems*, 2012, pp. 1097–1105.
- [8] M. Cimpoi, S. Maji, A. Vedaldi, Deep filter banks for texture recognition and segmentation, in: *Proceedings of the IEEE Conference on Computer Vision and Pattern Recognition*, 2015, pp. 3828–3836.
- [9] M. Cimpoi, S. Maji, I. Kokkinos, A. Vedaldi, Deep filter banks for texture recognition, description, and segmentation, *Int. J. Comput. Vis.* 118 (1) (2016) 65–94.
- [10] V. Andrarczyk, P.F. Whelan, Using filter banks in convolutional neural networks for texture classification, *Pattern Recognit. Lett.* 84 (2016) 63–69.
- [11] L. Liu, P. Fieguth, X. Wang, M. Pietikainen, D. Hu, Evaluation of LBP and deep texture descriptors with a new robustness benchmark, in: *European Conference on Computer Vision*, Springer, 2016, pp. 69–86.
- [12] T.-H. Chan, K. Jia, S. Gao, J. Lu, Z. Zeng, Y. Ma, PCANet: a simple deep learning baseline for image classification? *IEEE Trans. Image Process.* 24 (12) (2015) 5017–5032.
- [13] R.L. Kashyap, A. Khotanzad, A model-based method for rotation invariant texture classification, *IEEE Trans. Pattern Anal. Mach. Intell.* 4 (1986) 472–481.
- [14] J.-L. Chen, A. Kundu, Rotation and gray scale transform invariant texture identification using wavelet decomposition and hidden Markov model, *IEEE Trans. Pattern Anal. Mach. Intell.* 16 (2) (1994) 208–214.
- [15] H. Deng, D.A. Clausi, Gaussian MRF rotation-invariant features for image classification, *IEEE Trans. Pattern Anal. Mach. Intell.* 26 (7) (2004) 951–955.
- [16] J. Mao, A.K. Jain, Texture classification and segmentation using multiresolution simultaneous autoregressive models, *Pattern Recognit.* 25 (2) (1992) 173–188.
- [17] M. Varma, R. Garg, Locally invariant fractal features for statistical texture classification, in: *IEEE 11th International Conference on Computer Vision, 2007. ICCV 2007*, IEEE, 2007, pp. 1–8.
- [18] L. Liu, P. Fieguth, Texture classification from random features, *IEEE Trans. Pattern Anal. Mach. Intell.* 34 (3) (2012) 574–586.
- [19] J. Han, K.-K. Ma, Rotation-invariant and scale-invariant Gabor features for texture image retrieval, *Image Vis. Comput.* 25 (9) (2007) 1474–1481.
- [20] J. Zhang, M. Marszałek, S. Lazebnik, C. Schmid, Local features and kernels for classification of texture and object categories: a comprehensive study, *Int. J. Comput. Vis.* 73 (2) (2007) 213–238.
- [21] C.-H. Yao, S.-Y. Chen, Retrieval of translated, rotated and scaled color textures, *Pattern Recognit.* 36 (4) (2003) 913–929.
- [22] H. Ji, X. Yang, H. Ling, Y. Xu, Wavelet domain multifractal analysis for static and dynamic texture classification, *IEEE Trans. Image Process.* 22 (1) (2013) 286–299.
- [23] Y. Xu, H. Ji, C. Fermüller, Viewpoint invariant texture description using fractal analysis, *Int. J. Comput. Vis.* 83 (1) (2009) 85–100.
- [24] Y. Xu, S. Huang, H. Ji, C. Fermüller, Scale-space texture description on sift-like textons, *Comput. Vis. Image Underst.* 116 (9) (2012) 999–1013.
- [25] M. Crosier, L.D. Griffin, Using basic image features for texture classification, *Int. J. Comput. Vis.* 88 (3) (2010) 447–460.
- [26] T. Ojala, M. Pietikäinen, D. Harwood, A comparative study of texture measures with classification based on featured distributions, *Pattern Recognit.* 29 (1) (1996) 51–59.
- [27] T. Ojala, M. Pietikäinen, T. Maenpää, Multiresolution gray-scale and rotation invariant texture classification with local binary patterns, *IEEE Trans. Pattern Anal. Mach. Intell.* 24 (7) (2002) 971–987.
- [28] M. Pietikäinen, A. Hadid, G. Zhao, T. Ahonen, *Computer Vision Using Local Binary Patterns*, Computational Imaging and Vision, vol. 40, Springer Science & Business Media, 2011.
- [29] S. Liao, M.W. Law, A.C. Chung, Dominant local binary patterns for texture classification, *IEEE Trans. Image Process.* 18 (5) (2009) 1107–1118.
- [30] Z. Guo, L. Zhang, D. Zhang, Rotation invariant texture classification using LBP variance (LBPV) with global matching, *Pattern Recognit.* 43 (3) (2010) 706–719.
- [31] X. Huang, S.Z. Li, Y. Wang, Shape localization based on statistical method using extended local binary pattern, in: *Third International Conference on Image and Graphics (ICIG'04)*, IEEE, 2004, pp. 184–187.

- [32] X. Tan, B. Triggs, Enhanced local texture feature sets for face recognition under difficult lighting conditions, *IEEE Trans. Image Process.* 19 (6) (2010) 1635–1650.
- [33] S.R. Dubey, S.K. Singh, R.K. Singh, Rotation and illumination invariant interleaved intensity order-based local descriptor, *IEEE Trans. Image Process.* 23 (12) (2014) 5323–5333.
- [34] S.R. Dubey, S.K. Singh, R.K. Singh, Local wavelet pattern: a new feature descriptor for image Retrieval in medical CT databases, *IEEE Trans. Image Process.* 24 (12) (2015) 5892–5903.
- [35] S.R. Dubey, S.K. Singh, R.K. Singh, Multichannel decoded local binary patterns for content-based image retrieval, *IEEE Trans. Image Process.* 25 (9) (2016) 4018–4032.
- [36] Z. Li, G. Liu, Y. Yang, J. You, Scale- and rotation-invariant local binary pattern using scale-adaptive texton and subuniform-based circular shift, *IEEE Trans. Image Process.* 21 (4) (2012) 2130–2140.
- [37] E. Hayman, B. Caputo, M. Fritz, J.-O. Eklundh, On the significance of real-world conditions for material classification, in: European Conference on Computer Vision, Springer, 2004, pp. 253–266.
- [38] S. Lazebnik, C. Schmid, J. Ponce, A sparse texture representation using local affine regions, *IEEE Trans. Pattern Anal. Mach. Intell.* 27 (8) (2005) 1265–1278.
- [39] J. Serra, *Image Analysis and Mathematical Morphology*, vol. 1, Academic Press, 1982.
- [40] S. Mukhopadhyay, B. Chanda, Multiscale morphological segmentation of gray-scale images, *IEEE Trans. Image Process.* 12 (5) (2003) 533–549.
- [41] P. Maragos, Pattern spectrum and multiscale shape representation, *IEEE Trans. Pattern Anal. Mach. Intell.* 11 (7) (1989) 701–716.
- [42] K. Falconer, *Fractal Geometry: Mathematical Foundations and Applications*, John Wiley & Sons, 2004.
- [43] R. Van Den Boomgaard, A. Smeulders, The morphological structure of images: the differential equations of morphological scale-space, *IEEE Trans. Pattern Anal. Mach. Intell.* 16 (11) (1994) 1101–1113.
- [44] P.T. Jackway, Morphological scale-space, in: Proceedings 11th IAPR International Conference on Pattern, vol. III. Conference C: Image, Speech and Signal Analysis, IEEE Recognition, 1992, pp. 252–255.
- [45] J.G. Schavemaker, M.J. Reinders, J.J. Gerbrands, E. Backer, Image sharpening by morphological filtering, *Pattern Recognit.* 33 (6) (2000) 997–1012.
- [46] D.G. Lowe, Distinctive image features from scale-invariant keypoints, *Int. J. Comput. Vis.* 60 (2) (2004) 91–110.
- [47] R. Mehta, K. Egiazarian, Dominant rotated local binary patterns (DRLBP) for texture classification, *Pattern Recognit. Lett.* 71 (2016) 16–22.
- [48] S.K. Roy, B. Chanda, B.B. Chaudhuri, S. Banerjee, D.K. Ghosh, S.R. Dubey, Local directional ZigZag pattern: a rotation invariant descriptor for texture classification, *Pattern Recognit. Lett.* 108 (2018) 23–30.
- [49] W. Li, E.W. Tramel, S. Prasad, J.E. Fowler, Nearest regularized subspace for hyperspectral classification, *IEEE Trans. Geosci. Remote Sens.* 52 (1) (2014) 477–489.
- [50] R.A. Willoughby, Solutions of ill-posed problems (A.N. Tikhonov and V.Y. Atsnim), Society for Industrial and Applied Mathematics, SIAM Rev. 21 (2) (1979) 266–267.
- [51] K.J. Dana, B. Van Ginneken, S.K. Nayar, J.J. Koenderink, Reflectance and texture of real-world surfaces, *ACM Trans. Graph.* 18 (1) (1999) 1–34.
- [52] B. Caputo, E. Hayman, P. Mallikarjuna, Class-specific material categorisation, in: Tenth IEEE International Conference on Computer Vision, 2005. ICCV 2005, Vol. 2, IEEE, 2005, pp. 1597–1604.
- [53] S.K. Roy, B. Chanda, B.B. Chaudhuri, D.K. Ghosh, S.R. Dubey, A complete dual-cross pattern for unconstrained texture classification, in: Fourth IAPR Asian Conference on Pattern Recognition, ACPR 2017, IEEE, 2017, pp. 741–746.
- [54] A. Fathi, A.R. Naghsh-Nilchi, Noise tolerant local binary pattern operator for efficient texture analysis, *Pattern Recognit. Lett.* 33 (9) (2012) 1093–1100.
- [55] L. Liu, Y. Long, P.W. Fieguth, S. Lao, G. Zhao, BRINT: binary rotation invariant and noise tolerant texture classification, *IEEE Trans. Image Process.* 23 (7) (2014) 3071–3084.
- [56] M. Varma, A. Zisserman, A statistical approach to texture classification from single images, *Int. J. Comput. Vis.* 62 (1–2) (2005) 61–81.
- [57] M. Varma, A. Zisserman, A statistical approach to material classification using image patch exemplars, *IEEE Trans. Pattern Anal. Mach. Intell.* 31 (11) (2009) 2032–2047.
- [58] K. Wang, C.-E. Bichot, C. Zhu, B. Li, Pixel to patch sampling structure and local neighboring intensity relationship patterns for texture classification, *IEEE Signal Process. Lett.* 20 (9) (2013) 853–856.
- [59] Y. Xu, H. Ji, C. Fermuller, A projective invariant for textures, in: 2006 IEEE Computer Society Conference on Computer Vision and Pattern Recognition, Vol. 2, IEEE, 2006, pp. 1932–1939.
- [60] Z. Guo, X. Wang, J. Zhou, J. You, Robust texture image representation by scale selective local binary patterns, *IEEE Trans. Image Process.* 25 (2) (2016) 687–699.
- [61] F. Anscombe, The validity of comparative experiments, *J. R. Stat. Soc. A, General* 111 (3) (1948) 181–211.
- [62] F.J. Massey Jr., The Kolmogorov-Smirnov test for goodness of fit, *J. Am. Stat. Assoc.* 46 (253) (1951) 68–78.
- [63] J. Bruna, S. Mallat, Invariant scattering convolution networks, *IEEE Trans. Pattern Anal. Mach. Intell.* 35 (8) (2013) 1872–1886.
- [64] L. Sifre, S. Mallat, Rotation, scaling and deformation invariant scattering for texture discrimination, in: Proceedings of the IEEE Conference on Computer Vision and Pattern Recognition, 2013, pp. 1233–1240.



Swalpa Kumar Roy received both his Bachelor and Master degree in Computer Science & Engineering from West Bengal University of Technology, Kolkata, India, in 2012, and Indian Institute of Engineering Science and Technology, Shibpur, Howrah, India, in 2015. He is pursuing the Ph.D. degree under the Department of Computer Science & Engineering, University of Calcutta, Kolkata, India. He also works as a Project Linked Person under Computer Vision and Pattern Recognition unit, Indian Statistical Institute, Kolkata, India, from July 2015 to March 2016. He is currently working as an Assistant Professor in the Department of Computer Science & Engineering, Jalpaiguri Government Engineering College, Jalpaiguri, West Bengal, India. His research interests include Computer Vision, Computation Biology, Deep Learning, Image Processing, Texture Feature Description, Fractal Image Coding.



Bhabatosh Chanda received the B.E. degree in Elec. & Telecomm. Engg. and the Ph.D. degree in Electrical Engg. from the University of Calcutta, India, in 1979 and 1988, respectively. He is a Professor with the Indian Statistical Institute, Kolkata. Prof. Chanda received the Young Scientist Medal of the Indian National Science Academy, in 1989, the Vikram Sarabhai Research Award, in 2002, and the IETE-Ram Lal Wadhwa Gold Medal, in 2007. He has published a book titled *Digital Image Processing and Analysis* (Prentice-Hall India Learning, 2004). He is a fellow of the Institute of Electronics and Telecommunication Engineers, the National Academy of Science, India, the Indian National Academy of Engineering, and the International Association of Pattern Recognition (IAPR). His research interests include morphological image analysis, image texture segmentation, pattern recognition and image coding.



Bidyut B. Chaudhuri received his B.Sc. (Hons), B.Tech. and M.Tech. degrees from Calcutta University, India, in 1969, 1972 and 1974, respectively, and Ph.D. degree from Indian Institute of Technology, Kanpur, in 1980. He joined Indian Statistical Institute, in 1978 where he served as the Project Co-ordinator and Head of National Nodal Center for Knowledge Based Computing. Currently, he is the Head of Computer Vision and Pattern Recognition Unit of the institute. He has published more than 150 research papers in reputed International Journals and has authored a book titled *Two Tone Image Processing and Recognition* (Wiley Eastern, New Delhi, 1993). He is a fellow of the Institute of Electronics and Electrical Engineers (IEEE), the National Academy of Science, India, the Indian National Academy of Engineering, and the International Association of Pattern Recognition (IAPR). His research interests include Pattern Recognition, Image Processing, Computer Vision, Natural Language Processing and Digital Document Processing including OCR. He is serving as a associate editor of the journals *Pattern Recognition* and *Vivek* as well as guest editor of a special issue of *Journal IETE on Fuzzy Systems*.



Dipak Kumar Ghosh received the B.Tech. degree in Electronics and Communication Engineering from Kalyani Government Engineering College, in 2005, and M.Tech. degree in Mechatronics from Department of Electrical Engineering, National Institute of Technical Teachers' Training Research Kolkata, in 2009, under the West Bengal University of Technology, India. He received the Ph.D. degree in Gesture Recognition and Image Processing from National Institute of Technology Rourkela, India, in 2017. He is an Assistant Professor in the Department of Electronics and Communication Engineering, Adamas University, West Bengal, India. His research interest includes Signal and Image Processing, Texture Classification, Gesture Recognition, Pattern Recognition and Computer Vision.



Shiv Ram Dubey has been with the Indian Institute of Information Technology, SriCity (IIIT SriCity), since June 2016, where he is currently the Assistant Professor of Computer Science and Engineering. He received the Ph.D. degree in Computer Vision and Image Processing from Indian Institute of Information Technology, Allahabad (IIIT Allahabad), in 2016. Based on his Ph.D. research work, he published 10 SCI Journal papers including 5 IEEE Transactions/Journals. Before that, from August 2012 to Feb. 2013, he was a Project Officer in the

Computer Science and Engineering Department at Indian Institute of Technology, Madras (IIT Madras). He was a recipient of several awards including the Early Career Research Award from SERB, Govt. of India and NVIDIA GPU Grant from NVIDIA. He received Certificate of Reviewing Awards from Biosystems Engineering and Computers in Biology and Medicine, Elsevier, in 2015 and 2016, respectively. He received the Best Paper Award in IEEE UPCON 2015, a prestigious conference of IEEE UP Section. His research interest includes Computer Vision, Deep Learning, Image Processing, Image Feature Description, Image Matching, Content Based Image Retrieval, Medical Image Analysis and Biometrics.